Application of 1D iFEM to an Experimental Beam Model with Degrading Boundary Conditions

JACOPO BARDIANI, FRANCESCO ORSENIGO, ANDREA MANES and CLAUDIO SBARUFATTI

Jacopo Bardiani, Politecnico di Milano, via La Masa 1, 20156, Milano, Italy Francesco Orsenigo, Politecnico di Milano, via La Masa 1, 20156, Milano, Italy
Andrea Manes, Politecnico di Milano, via La Masa 1, 20156, Milano, Italy
Claudio Sbarufatti, Politecnico di Milano, via La Masa 1, 20156, Milano, Italy
Corresponding author: jacopo.bardiani@polimi.it (Jacopo Bardiani)

ABSTRACT

The inverse Finite Element Method (iFEM) is a robust computational technique that utilizes a network of strain sensors to reconstruct full-field displacement on beam or shell structures. Importantly, the method is independent of specific loading conditions and material properties, making it particularly suitable for real-time structural monitoring and assessment. By providing a comprehensive understanding of structural behaviour, iFEM enables the implementation of condition-based maintenance policies, which are crucial for enhancing the operational lifespan of engineering structures. This study evaluates for the first time the effectiveness of 1D iFEM strategy in shape sensing of an experimental beam structure with degrading boundary conditions. In addition, a dedicated procedure has been implemented to reconstruct the percentage reduction in the stiffness of the degraded constraint, which is essential for structural health monitoring and for defining appropriate retrofitting strategies to be applied to the structure. The results show the potential of iFEM for structural health monitoring and adaptive maintenance strategies in real-world applications, where boundary conditions may evolve over time.

INTRODUCTION

Infrastructures failure stems from material deterioration mechanisms and human and operational factors such as design errors, construction flaws, and overloading [1]. Moreover, multiple deterioration mechanisms, both physical and chemical, can act simultaneously and significantly compromise the infrastructure's durability and structural integrity, becoming also difficult to model. In this context, deflection monitoring becomes a key aspect of bridge Structural Health Monitoring (SHM), as deflection data can reveal early signs of structural anomalies [2,3]. Among possible causes of damage, chloride-induced corrosion of steel reinforcement is particularly critical, leading to cracking, and eventually resulting in the loss of bond and cross-sectional capacity of the steel, thereby reducing the service life of the structure [4]. In addition, pier scour, defined as the erosion of soil around bridge foundations caused by flowing water, is a leading cause of structural collapse in flood-prone regions. It induces vertical settlements and rotational displacements at the foundation level, which can trigger extensive structural damage [5].

However, conventional monitoring techniques often rely on fixed reference points, which may be unstable and are typically expensive to maintain [2,3]. To overcome these limitations, reference-free approaches have emerged, utilizing various sensors such as tiltmeters [2], accelerometers [7], satellites [8], and strain gauges [9]. Among them, fiber optic strain sensors are particularly promising due to their ability to perform distributed measurements along the structure [10–12]. While some studies have successfully estimated deflections from strain data [2,9,13], they often depend on auxiliary systems (e.g., tiltmeters or sensing bars) or require detailed knowledge of material properties, which can limit real-world applicability. These challenges can be addressed using the inverse Finite Element Method (iFEM), which reconstructs deflections solely from distributed fiber optic strain measurements installed directly on the bridge girder.

However, a critical limitation that has received little attention in the literature arises precisely from the fact that, corrosion and scour, for example, may alter the effective

support conditions and boundary constraints of the bridge system over time, rendering the initial boundary condition assumptions of the model invalid. Although iFEM is independent of the material properties and external loads of the structure, it still relies on an accurate definition of the boundary conditions to produce reliable reconstructions. When these boundary conditions are uncertain or unknowingly changed due to deterioration, the accuracy of the deflection estimation deteriorates accordingly.

This situation, where the boundary conditions are completely unknown, can frequently arise in both civil and other types of structures. Another paradigmatic example is reinforced concrete spatial frames made up of beams and columns. If we consider a typical beam placed between two columns, the boundary conditions initially applied to the beam are perfectly fixed support. However, over the life cycle of the structure, these supports gradually degrade due to creep, fatigue, and other similar effects, causing the boundary condition to transition from a perfect fixity to partial fixity. The rotational stiffness of this partial fixity remains entirely unknown.

This phenomenon is extremely critical in the context of structural monitoring using the iFEM strategy, as it introduces additional uncertainties to the problem, which must be addressed to accurately reconstruct the displacement field. This work presents, for the first time, a framework in which iFEM addresses the issue of degrading conditions. The framework is applied to a simple aluminum beam, where numerical simulations of strain are provided as input to iFEM. Two different configurations are considered, each characterized by a distinct level of degradation in the boundary condition.

The new framework, which is still in its preliminary stages, demonstrates highly promising results and strongly emphasizes the need for deeper exploration into these critical issues. This initial success underscores the importance of advancing the research to fully understand and address the challenges associated with degrading boundary conditions, paving the way for more robust and accurate structural monitoring approaches in the future.

METHODOLOGY

The structure can be discretized with N inverse beam elements, making use of the zero-order Euler-Bernoulli inverse beam elements developed in [14,15]. An illustration of the element with the coordinate system and the degrees of freedom (DOF) is depicted in Figure 1. Each beam element is defined by a local reference system with the z axis coinciding with the longitudinal axis of the beam, with the x and y axes representing the section's principal axes of inertia. The element length is L_e, the section area is A_e and the moments of inertia about the principal axes are I_x^e and I_y^e.

Neglecting torsional effects, the beam kinematics are fully described by a displacement vector containing the displacements of the neutral axis along the z, y, and x directions, and the rotations of the cross section about the x and y axes, as shown in Figure 1. Since torsion is excluded from the model, rotation about the z-axis is not considered, and shear strain components are assumed to be zero. The non-zero strain component includes only axial deformation and bending contributions in the xz and yz planes. These components, referred to as section strains, are collectively expressed in the strain vector $\boldsymbol{e}$.

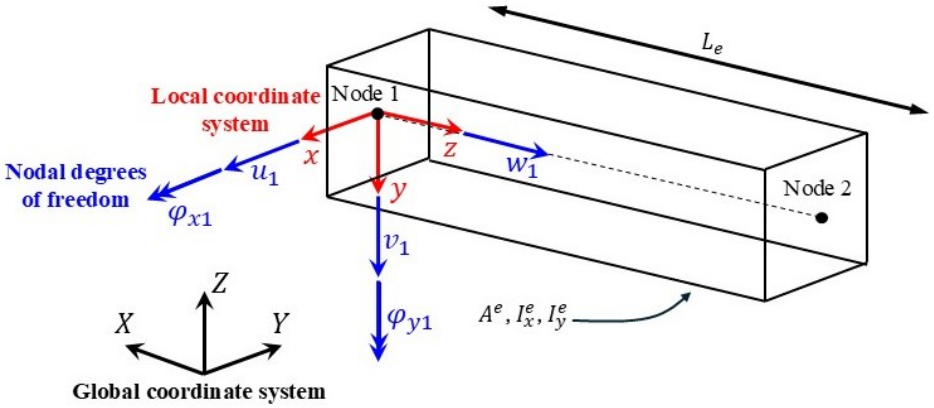

Figure 1. Illustration of an iFEM element with local and global coordinate systems.

To reconstruct the displacement field from experimentally measured section strains, the least-square functional $\Phi(\boldsymbol{u}, \boldsymbol{e}_e^{\boldsymbol{\varepsilon}})$ is formulated for each inverse element. It consists in the Euclidean norm of the error between the section strains according to the Euler-Bernoulli beam theory $\boldsymbol{e}(\boldsymbol{u})$ and the experimentally measured strains $\boldsymbol{e}_e^{\boldsymbol{\varepsilon}}$. This can be expressed as follows:

$$\Phi_e(\boldsymbol{u}) = \|\boldsymbol{e}(\boldsymbol{u}) - \boldsymbol{e}_e^{\boldsymbol{\varepsilon}}\|^2 \tag{1}$$

The contribution of each element is then summed over in the functional Φ. The nodal displacements $\boldsymbol{u}$ are computed by minimizing the Φ.
The contribution of each element functional is expanded by making use of the definition of the strain vector. Axial strains are considered negligible due to the free movement of the roller supports and longer spans, magnifying the role of flexural strains compared to other strains in this bridge. Additionally, the flexural contribution χ_y in the horizontal plane cannot be considered because there are no placed sensors able to measure the deflection in that direction. Therefore, the overall equation of the functional can be simplified as follows:

$$\Phi_e(\boldsymbol{u}) = \frac{L^e \cdot I_x^e}{n_e \cdot A^e} \cdot \sum_{i=1}^{n_e} \left(\chi_x(z_i) - \chi_{x_i}^m\right)^2 \tag{2}$$

Where n_e are the number of strain measurements for the element e, and i indexes the strain measurements in the element, which are provided at the locations z_i. The term $\chi_x(z_i)$ is the section strain of the iFEM model evaluated at the location z_i, while $\chi_{x_i}^m$ is the experimentally measured strain at z_i. All the measured strains contained in the spatial domain of the element are input into the iFEM algorithm.
Consistently with the small strain hypothesis, Eq. (2) can be expressed in terms of the nodal degrees of freedom contained in the vector $\boldsymbol{u_e}$, as follows:

$$\Phi_e(\boldsymbol{u}) = \frac{1}{2}\boldsymbol{u_e}^T \cdot \boldsymbol{k_e} \cdot \boldsymbol{u_e} - \boldsymbol{u_e}^T \cdot \boldsymbol{f_e} + c \tag{3}$$

Noted that the $\boldsymbol{k_e}$ is a constant matrix and only depends on the geometry of the element, while the $\boldsymbol{f_e}$ is a column vector that depends on the measured strain data $\boldsymbol{\varepsilon}_i$. The functional for each element $\Phi_e(\boldsymbol{u})$ can then be transformed from the local coordinate system (x, y, z) to the global coordinate system (X, Y, Z) using standard transformation matrices for finite elements and minimized with respect to the nodal degrees of freedom $\boldsymbol{u_e}$. Finally, the contribution of each element can then be assembled in a global linear system of equations with the degrees of freedom of all the nodes:

$$\boldsymbol{K^G} \cdot \boldsymbol{u^G} = \boldsymbol{f^G} \tag{4}$$

Where the superscript G denotes the matrices and vectors transformed into the global coordinate system.

Boundary conditions can then be applied via Lagrange multipliers or penalty method, as in any standard FE problem. The resulting linear system of equations is nonsingular when the strain measurement locations of one element are more than two [14]. With the matrix $\boldsymbol{K^G}$ given by the structural geometry and $\boldsymbol{f^G}$ given by the measured surface strain $\boldsymbol{\varepsilon}_i$, the nodal deflection of the structure can be calculated by solving $\boldsymbol{u^G}$ from the linear system of equation. Once the nodal deflection is known, the deflection at any point in the structure can be computed through the shape functions of the elements. Since the only strain-dependent term is $\boldsymbol{f^G}$, the matrix $\boldsymbol{K^G}$ may be inverted only once. Therefore, the method has the potential to be applied online in real time, at a minimal computational cost, independently of the applied loads and structural dynamics. For a more comprehensive understanding, readers are encouraged to consult [14-16] for an in-depth exploration of how this method functions.

Applying the penalty method involves introducing penalty terms into the system, which act as stiffness coefficients of virtual springs enforcing boundary conditions. However, unlike in classical structural theory, where stiffness is typically expressed in units such as N/m or Nm/rad, the unit conventions adopted in the iFEM stiffness matrix differ, being tailored to the method's specific formulation. As a result, these penalties cannot be directly interpreted as physical spring stiffnesses. Similarly, when boundary conditions are enforced using Lagrange multipliers, they should not be interpreted as reaction forces or moments, but just as mathematical variables used to impose constraints within the system. These penalties modify the stiffness matrix to approximate constrained behaviour without explicitly imposing displacement constraints. To solve the linear system using this approach, appropriate penalty values must be defined. The key challenge lies in determining the optimal penalties such that the resulting displacements are consistent with the actual structural response. To this end, the stiffness matrix is augmented by adding penalty terms to all N_c constrained degrees of freedom at specific evaluation instants (ei) defined by the monitoring strategy, as expressed in the following equation:

$$\boldsymbol{K_{new}^{ei}} = \boldsymbol{K}_0 + \sum_{i=1}^{N_c} \lambda_i^{ei} \cdot \boldsymbol{E}_i \quad , \forall ei = t_1, t_2, \dots \tag{5}$$

The objective then becomes the minimization of a residual function $r(\cdot)$, which depends on the augmented stiffness matrix defined in Eq. (5):

$$\min r(\boldsymbol{K}_{\boldsymbol{new}}^{ei}) \tag{6}$$

The percentage reduction in stiffness associated with a specific DOF i (in the specific case of the present study φ_x) can be quantified using the above expression, where $k_i^{t_1}$ and $k_i^{t_2}$ represent the values of the corresponding diagonal term in the global stiffness matrix at two different time steps or degradation states. This formulation isolates the contribution of the penalty stiffness imposed on the selected DOF, allowing for a direct comparison of its degradation over time.

$$\Delta k_i^{\%} = 100 \cdot \frac{k_i^{t_2} - k_i^{t_1}}{k_i^{t_1}} \tag{7}$$

CASE STUDY

In the present paragraph, a brief description of the case under investigation is discussed, with a focus on the direct model of the aluminum beam, on the sensor network and on the inverse FE model.

The direct FEM

To validate the proposed framework, the geometry of a simple aluminum beam was adopted, featuring a rectangular cross-section with a base of 50 mm and a height of 10 mm, and a support span of 648 mm. The aluminum has the following mechanical properties: Young's modulus E equal to 70 GPa and Poisson's ratio υ equal to 0.3. Two numerical models of the aluminum beam were developed in ABAQUS CAE (version 6.23), each consisting of 648 B23 beam elements. The loading condition considered consists of a single concentrated force applied at midspan, with an intensity of F equal to 294.3 N, corresponding to a mass of 30 kg. The models differ in the imposed boundary conditions, as described in the previous section, to simulate two distinct structural configurations corresponding to different stages of the beam's operational life. The boundary conditions that have been considered are as follows: in the first model, a rotational spring with stiffness k_{ϑ,t_1} equal to 25516300 Nm/rad is applied at one end of the beam (left), while the other end (right) is fully clamped. In the second model, the same configuration is maintained, but the rotational spring has a reduced stiffness k_{ϑ,t_1} equal to 931256 Nm/rad. These two direct models represent two generic instants in the operational life of the structure, with the second configuration simulating a more degraded condition of the support, in which its rotational stiffness has decreased over time, from 0.05° to 0.5°. The theoretical change in boundary stiffness in the FEM model corresponds to a reduction of approximately 96.35%. The two configurations described above are illustrated in Figure 2.
The two simulations described in this section are required to extract the strain values $\boldsymbol{\varepsilon}_{in}$ to be used as input for the iFEM code, in accordance with the sensor network configuration presented in the following section.

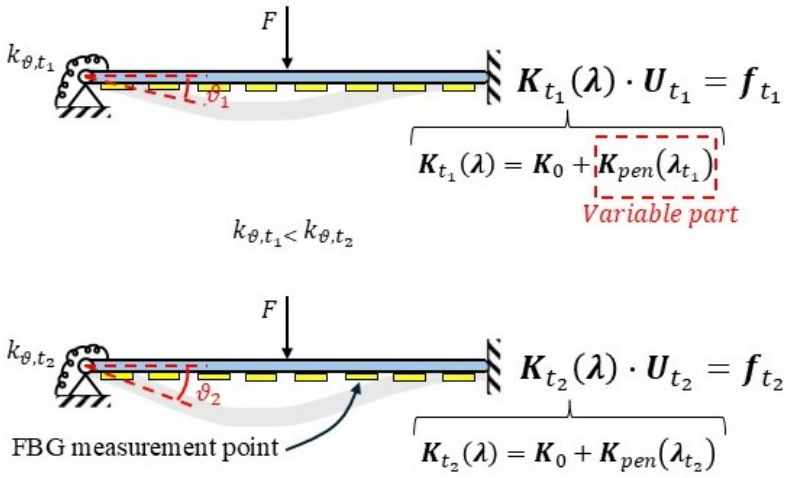

Figure 2. Schematic representation of the two direct FE models implemented in ABAQUS CAE.

The sensor network

A Fiber Bragg Grating (FBG)-based sensor network was assumed, following the layout depicted in Figure 3. The network consists of 18 measurement points (indicated by red marks), spaced 36 mm apart. The same figure also illustrates the design of a potential FBG sensor network that could be implemented under real operating conditions of the aluminum beam.

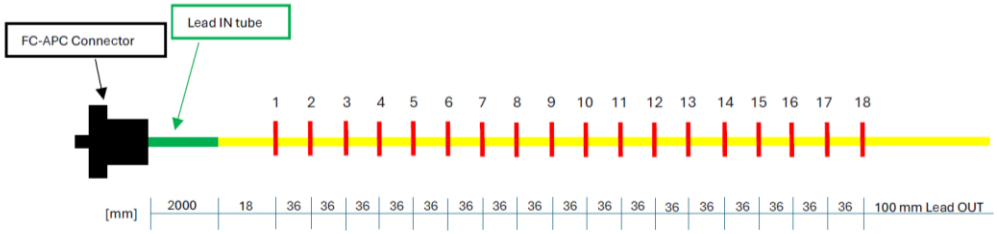

Figure 3. FBG-based sensor network layout considered for the beam of the present study.

The presented sensor network was assumed to be positioned along the centerline of the bottom surface of the beam and was bonded starting from the transition point between the green and yellow segments (refer to the schematic representation of Figure 3). This sensor network configuration was chosen for its simplicity of implementation, reduced number of sensing points, and compatibility with standard FBG interrogation systems. Moreover, its placement along the centerline of the bottom surface allows for effective capture of the maximum strain values typically occurring under bending, while minimizing installation complexity and optical fiber routing issues. The strain values from the direct FEM simulations were extracted at locations corresponding to the sensing points of the FBG-based sensor network, ensuring consistency between the numerical and experimental data acquisition schemes.

The inverse FE model

The iFEM model of the beam consists of nine 1D inverse finite elements based on the Euler-Bernoulli formulation. Each element has a length L_e of 72 mm, corresponding to a uniform discretization over the total beam length of 648 mm. According to the formulation of the 0th-order Euler-Bernoulli inverse finite element, two measurement points are defined within each element. These are symmetrically positioned at one-quarter and three-quarters of the element length, i.e., at local coordinates $\xi = 0.25 \cdot L_e$ and $\xi = 0.75 \cdot L_e$ (with ξ local coordinate of the inverse element), to provide optimal strain information for reconstructing the section strain components. An important aspect to be mentioned regarding the inverse models developed in this study concerns the implementation of the boundary conditions. Specifically, for the non-degraded end of the beam (on the right), the inverse model assumes a fully clamped boundary condition. In contrast, for the support subject to degradation, rotational spring stiffness is not known as a priori. Therefore, a hinge boundary condition was applied in the inverse model to allow free rotation, while an imposed rotation was introduced as a known quantity, estimated from the full set of strain measurements.

RESULTS AND DISCUSSION

The displacement field reconstruction for the beam under the two considered boundary conditions is shown in Figure 2. As observed, the previously described procedure yields excellent agreement between the iFEM reconstruction and the numerical reference solution, both along the entire beam and in the regions affected by BC degradation. Moreover, the application of Eq. (7) resulted in a computed stiffness reduction of approximately 91.22%, which is close to the exact theoretical value of 96.35%.

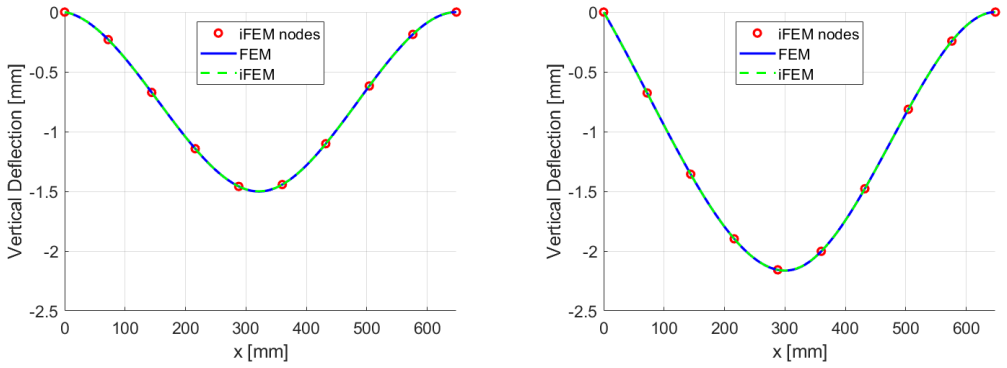

(a) (b)

Figure 3. Displacement reconstruction provided by the iFEM for the two degraded boundary conditions shown in Figure 2: (a) left BC with k_{ϑ,t_1} and (b) left BC with k_{ϑ,t_2}.

CONCLUSIONS

This study demonstrated the capability of 1D iFEM to accurately reconstruct displacement fields in beam structures with degraded boundary conditions. The results showed excellent agreement with FEM simulations for both degradation levels, and the

penalty-based approach provided a reliable estimation of the stiffness reduction. These outcomes confirm the potential of iFEM as a powerful tool for structural health monitoring in scenarios where boundary conditions evolve over time.

REFERENCES

1. Zhang, G., Liu, Y., Liu, J., Lan, S., and Yang, J. 2022. "Causes and statistical characteristics of bridge failures: A review". *Journal of Traffic and Transportation Engineering (English Edition)*, 9(3), 388–406. https://doi.org/10.1016/j.jtte.2021.12.003
2. Helmi, K., Taylor, T., Zarafshan, A., and Ansari, F. 2015. "Reference free method for real time monitoring of bridge deflections". *Engineering Structures*, 103:116-124. https://doi.org/10.1016/j.engstruct.2015.09.002
3. Wang, C., Ansari, F., Wu, B., Li, S., Morgese, M., and Zhou, J. 2022. "LSTM approach for condition assessment of suspension bridges based on time-series deflection and temperature data". *Advances in Structural Engineering*, 25(16):3450-3463. https://doi.org/10.1177/13694332221133604
4. Penttala, V. 2009. "Causes and mechanisms of deterioration in reinforced concrete". In *Failure, distress and repair of concrete structures*, edited by N. Delatte, 3–31. First Edition. Woodhead Publishing Limited. https://doi.org/10.1533/9781845697037.1.3
5. Zampieri, P., M. A. Zanini, F. Faleschini, L. Hofer, and C. Pellegrino. 2017. "Failure analysis of masonry arch bridges subject to local pier scour". *Engineering Failure Analysis* 79: 371–384. https://doi.org/10.1016/j.engfailanal.2017.05.028
6. Kefal, A., Oterkus, E., Tessler, A., & Spangler, J. L. 2016. "*A quadrilateral inverse-shell element with drilling degrees of freedom for shape sensing and structural health monitoring*". *Engineering science and technology, an international journal*, 19(3):1299-1313. https://doi.org/10.1016/j.jestch.2016.03.006
7. Moreu, F., Chen, L., Zhu, C., Wu, Z., Yuan, X. 2023. "Measuring Total Transverse Reference-Free Displacements of Railroad Bridges Using Two Degrees of Freedom: Experimental Validation". Journal of Infrastructure Systems, 29, 04023009. https://doi.org/10.1061/JITSE4.ISENG-2132.
8. Stiros, S.C. 2021. "GNSS (GPS) Monitoring of Dynamic Deflections of Bridges: Structural Constraints and Metrological Limitations". Infrastructures, 6, 23. https://doi.org/10.3390/infrastructures6020023
9. You, R.-Z., Yi, T.-H., Ren, L., Li, H.-N. 2023. "Equivalent Estimation Method (EEM) for Quasi-Distributed Bridge Deflection Measurement Using Only Strain Data". Measurement, 221, 113492. https://doi.org/10.1016/j.measurement.2023.113492
10. Ansari, F. 2007. "Practical Implementation of Optical Fiber Sensors in Civil Structural Health Monitoring". Journal of Intelligent Material Systems and Structures, 18, 879–889. https://doi.org/10.1177/1045389X06075760
11. Morgese, M., Ying, Y., Taylor, T., Ansari, F. 2022. "Method and Theory for Conversion of Distributed Fiber-Optic Strains to Crack Opening Displacements". Journal of Engineering Mechanics, 148, 04022072. https://doi.org/10.1061/(ASCE)EM.1943-7889.0002168
12. Morgese, M., Wang, C., Taylor, T., Etemadi, M., Ansari, F. 2024. "Distributed Detection and Quantification of Cracks in Operating Large Bridges". Journal of Bridge Engineering, 29, 04023101. https://doi.org/10.1061/JBENF2.BEENG-6454
13. Skafte, A., Aenlle, M.L., Brincker, R. 2016. "A General Procedure for Estimating Dynamic Displacements Using Strain Measurements and Operational Modal Analysis". Smart Materials and Structures, 25, 025020. https://doi.org/10.1088/0964-1726/25/2/025020
14. Savino, P. (2019). "Shape sensing with inverse finite element method for slender structures". *Structural Engineering and Mechanics, An Int'l Journal*, 72(2):217-227. https://doi.org/10.12989/SEM.2019.72.2.217
15. Gherlone, M., Cerracchio, P., Mattone, M., Di Sciuva, M., and Tessler, A. 2014. "An inverse finite element method for beam shape sensing: theoretical framework and experimental validation". *Smart Materials and Structures*, 23(4), 045027. https://doi.org/10.1088/0964-1726/23/4/045027
16. Poloni, D., Morgese, M., Wang, C., Taylor, T., Giglio, M., Ansari, F., and Sbarufatti, C. 2025. "Reference-free distributed monitoring of deflections in multi-span bridges". *Engineering Structures*, 323, 119277. https://doi.org/10.1016/j.engstruct.2024.119277